Innovative Food Science and Emerging Technologies 110 (2026) 104488

Contents lists available at ScienceDirect

Innovative Food Science and Emerging Technologies

journal homepage: www.elsevier.com/locate/ifset

Fabrication of small-sized starch nanoparticles and their inhibition of interfacial enzymatic hydrolysis of granular starch

Zhihang Li [a,b,1], Yu Tian [a,b,1], Jacob Judas Kain Kirkensgaard [c,d], Birte Svensson [e], Andreas Blennow [f,*], Yu Wang [e,g,*]

[a] Lab of Food Soft Matter Structure and Advanced Manufacturing, College of Food Science and Engineering, Nanjing University of Finance and Economics, Collaborative Innovation Center for Modern Grain Circulation and Safety, Nanjing 210023, China
[b] Department of Plant and Environmental Sciences, University of Copenhagen, DK-1871 Frederiksberg C, Denmark
[c] Department of Food Science, University of Copenhagen, DK-1958 Frederiksberg C, Denmark
[d] Niels Bohr Institute, University of Copenhagen, DK-2100 Copenhagen Ø, Denmark
[e] Enzyme and Protein Chemistry, Department of Biotechnology and Biomedicine, Technical University of Denmark, DK-2800 Kgs. Lyngby, Denmark
[f] School of Food Science and Technology, Jiangnan University, Wuxi, Jiangsu, 214222, China
[g] Department of Food Nutrition and Safety/National R&D Center for Chinese Herbal Medicine Processing, College of Engineering, China Pharmaceutical University, Nanjing 211198, China

ARTICLE INFO

Keywords:
Small-sized starch nanoparticles
Branching enzyme
Glucoamylase inhibition
Interfacial kinetics
Enzyme adsorption
Ternary complex

ABSTRACT

Starch nanoparticles (sNPs) are promising for glycemic control and bioactive delivery, yet achieving high-yield, sustainable production of ultra-small particles (<50 nm) with clarified inhibitory mechanisms against digestive enzymes remains a significant challenge. This study systematically addressed this gap by developing a scalable, sustainable fabrication method for ss-sNPs. It further elucidates how nanoparticle size and amylose content influence their interfacial inhibitory mechanisms against glucoamylase (GA). We produced ss-sNPs with a high yield (90%) using an environmentally friendly approach combining enzymatic modification and sonication. The ss-sNPs measuring 10–30 nm, derived from branching enzyme-treated potato starches of varying amylose content, exhibited stability for one week before swelling to 84–833 nm during storage. Notably, the ss-sNPs exhibited enhanced resistance to *in vitro* digestion by glucoamylase (GA). While the ss-sNPs (10–14 nm) from high amylopectin (waxy, WPS) and normal (NPS) potato starch non-competitively inhibited GA hydrolysis of wheat starch granules, larger ss-sNPs (30 nm) from high amylose starch (HPS) un-competitively inhibited GA weakly, indicating GA-sNPs ternary complex formation with granular surfaces. Interfacial kinetics and *Langmuir* binding analyses further revealed loss of GA attack and binding sites. This scalable and sustainable ss-sNPs fabrication strategy offers remarkable interfacial capabilities unlocking potential applications in the food and biotechnology sectors.

List of abbreviations

$^{abs}\Gamma_{max}$	Density of binding sites
A/B ratio	Attack site density/binding site density ratio
AP	Amylopectin
BE	Branching enzyme
CLD	Chain length distribution
DP	Degree of polymerization
DP_{ave}	Average degree of polymerization
FTIR-ATR	Fourier transform infrared-Attenuated total reflectance
GA	Glucoamylase
GOPOD	D-Glucose assay kit
HPAEC-PAD	High performance anion exchange chromatography with pulsed amperometric detection
HPS	High-amylose potato starch
HPS-NP	High-amylose potato starch nanoparticle
$^{inv}k_{cat}$	Turnover number from inverse MM-kinetics
k_{cat}	Turnover number from conventional MM-kinetics
K_d	Binding constant
$^{kin}\Gamma_{max}$	Density of attack sites

(continued on next column)
(continued)
(continued on next page)

* Corresponding authors.
E-mail addresses: andreas.blennow1@gmail.com (A. Blennow), yuwang@cpu.edu.cn (Y. Wang).
[1] These authors contributed equally to this work.

https://doi.org/10.1016/j.ifset.2026.104488
Received 7 January 2026; Received in revised form 9 February 2026; Accepted 9 February 2026
Available online 12 February 2026

(*continued*)

$K_{1/2}$	Mass load at substrate half-saturation from conventional MM-kinetics
MM	Michaelis-Menten
ns	non-significant
NPs	Nanoparticles
NPS	Normal potato starch
NPS-NP	Normal potato starch nanoparticle
PCL	Poly(*ε*-caprolactone)
PDI	Polydispersity index
PLA	Polylactide
PLGA	Poly- (lactide-*co*-glycolide)
RDS	Rapidly digested starch
RI	Refractive index
RS	Resistant starch
R_h	Hydro-dynamic radius
*Ro*BE	*Rhodothermus obamensis* branching enzyme
SDS	Slowly digested starch
SEC	Size exclusion chromatography
SEM	Scanning electron microscope
ss-sNPs	Small-sized starch nanoparticles
WAXS	Wide-angle X-ray scattering
$W(\log V_h)$	The molecular weight distribution based on the relationship between elution volume and hydrodynamic radius ($\log V_h$) for pullulan standards
WPS	Waxy potato starch
WPS-NP	Waxy potato starch nanoparticle
^{1}H NMR	Proton nuclear magnetic
4αGT	4-α-glucanotransferase.

1. Introduction

Nanoparticles (NPs) are predominantly characterized by their size, typically ranging from a few to several hundred nanometers (Rao & Geckeler, 2011). Compared to bulk materials, NPs exhibit an exceptionally high surface-to-volume ratio and enhanced reactivity, while providing unique optical and electrical properties (Mitchell et al., 2021; Rao & Geckeler, 2011). These characteristics enable their application across different technological fields, including bioimaging, catalysis, solar energy, light-emitting diodes, drug delivery, and the food, cosmetics, medicine, and agricultural industries (Erathodiyil & Ying, 2011; Flores et al., 2019; Goh et al., 2012; Kou, Faisal, Song, & Blennow, 2023; Salata, 2004). Interestingly, NPs can be applied as digestive inhibitors, thus silver NPs exhibit potent inhibitory activity against pancreatic α-amylase, although their practical application is restricted by their toxicity (Balan et al., 2016). However, certain NPs, such as metal-, metal oxide- and carbon-based NPs, may be cytotoxic and poorly biodegradable (Prasad & Selvaraj, 2024; Vieira, de Carvalho, & Conte-Junior, 2022). Therefore, development of safer NP systems is essential. Previous studies indicate that nanocrystalline cellulose- and starch-based NPs can inhibit α-amylase and α-glucosidase. However, their underlying mechanisms and functional potential require thorough characterization (Jiang, Li, Chang, Xiong, & Sun, 2018; Nsor-Atindana et al., 2019; Nsor-Atindana, Yu, Goff, Chen, & Zhong, 2020).

Commonly used polymers for NP fabrication include biodegradable polyesters like poly(*ε*-caprolactone) (PCL), polylactide (PLA), and poly (lactide-*co*-glycolide) (PLGA) (Da Costa et al., 2021; Fahimirad et al., 2021; Hamadani et al., 2023). Even though natural polymers such as cellulose, starch, and dextran have also been used, synthetic polymers are often preferred due to their higher purity and superior reproducibility (Chen et al., 2024; Deeksha, Sadanand, Hariram, & Rajulu, 2021; Hu, Lu, & Luo, 2021). Nevertheless, starch remains a candidate of high interest as it is an abundant, natural, biodegradable and renewable biopolymer harvested in substantial volumes from the seeds, grains, roots and tubers of various crops, mainly corn, potato, wheat, and rice (Li et al., 2023; Liu, Liu, Yu, Copeland, & Wang, 2023; Liu et al., 2025; Wang, Møller, & Svensson, 2024).

Starch consists of two α-glucan macromolecules, namely the essentially linear amylose of glucose residues connected by α-1,4-glucosidic linkages, and amylopectin containing 5–6% α-1,6-branching points in α-1,4-glucosidic stretches (Damager, Engelsen, Blennow, Lindberg Møller, & Motawia, 2010; Li et al., 2023; Sharanagat, Saxena, Kumar, & Kumar, 2023; Tian et al., 2023). Native granular starch is unsuitable for preparing NPs due to its semi-crystalline structure, low solubility, lack of additional reactive functionalities beyond hydroxyl groups, and the tendency to undergo retrogradation and aggregation after gelatinization, which hinders the formation of stable nanoscale particles (Le Corre, Bras, & Dufresne, 2010). Therefore, additional treatments, such as enzymatic modification, commonly by α-amylase, GA, and pullulanase, an α-1,6 debranching hydrolase (Campelo, Sant'Ana, & Clerici, 2020; Yan et al., 2022), are used to upgrade native starch for production of NPs. We previously prepared highly branched modified starches with hydrodynamic radius (R_h) < 10 nm using branching enzyme (BE) and 4-α-glucanotransferase (4αGT), which were suitable for preparing small-sized starch nanoparticles (ss-sNPs) (Chen, Wang, Tian, Svensson, & Blennow, 2024). In a different study we showed that ss-sNPs of about 20 nm were spontaneously crossing the plant cell wall barrier, and rapidly taken up by *Arabidopsis* roots, indicating potential for substance delivery in plants (Chen et al., 2024). However, the recovery of branched starch with R_h = 10–20 nm from native starches *via* nanoprecipitation resulted in very low (<10%) yields (Chen, Ding, et al., 2024).

Table 1
Characteristics of starch granules.

Starch type	Abbreviation	Amylose content (%)	Crystalline polymorph
Waxy potato starch	WPS	1.9	B-type
Normal potato starch	NPS	26.3	B-type
High-amylose/high-phosphate potato starch	HPS	35.2	B-type
Normal wheat starch	NWS	33.1	A-type

To address the challenge of low yield and further explore the functional potential of these nanostructures, the primary objective of this study is to develop a high-yield, scalable method for producing ss-sNPs. We hypothesize that enzymatic modification using *Rhodothermus obamensis* branching enzyme (*Ro*BE) combined with sonication will significantly enhance the yield of highly branched ss-sNPs compared to conventional methods. Furthermore, this work aims to explicitly characterize the interaction between the resulting ss-sNPs and digestive enzymes. Specifically, we investigate the hypothesis that these ss-sNPs can act as effective inhibitors of interfacial catalysis by GA on wheat starch granules. This study focuses on optimizing the fabrication process using three potato starch types with varying amylose contents and elucidating the mechanism behind their resistance to hydrolytic digestion.

2. Materials and methods

2.1. Materials

Three different potato starches were used for ss-sNPs preparation (Table 1). High amylopectin (waxy) potato starch (WPS), derived from an RNA interference granule bound starch synthase (GBSS) line, was a generous gift of Lyckeby Stärkelsen, Sweden. Normal potato starch (NPS) and high-amylose/high-phosphate potato starch (HPS) were isolated from the potato cultivar Dianella and a dual RNA interference branching enzyme (BE) I and II line in the Dianella genetic background, respectively, following established protocols (Blennow et al., 2005; Kozlov, Blennow, Krivandin, & Yuryev, 2007). Normal wheat starch (NWS) was a kind gift of Lantmännen, Sweden. BE from *Rhodothermus obamensis* (*Ro*BE, 5.98 U/mg) was generously supplied by Novozymes (Bagsværd, Denmark). Pullulanase M2 from *Bacillus licheniformis* (*Bl*Pul, *E*-PULBL, 900 U/mL, 12.8 mg/mL, Mw = 113,000 Da), as well as D-Glucose Assay Kit, and Total Starch Assay Kit (AA/AMG) were procured from Megazyme Co. Ltd. (Wicklow, Ireland). Trimethylsilylpropanoic

acid (TMSP), GA from *Aspergillus niger* (A7095, 260 U/mL) and pancreatin (P7545, 8 × USP) were purchased from Sigma-Aldrich Co. Ltd. (St. Louis, MO, USA).

2.2. Preparation of ss-sNPs

Dry starch powder (6%, w/v) was suspended in 50 mM MES buffer containing 150 mM NaCl (pH 6.0), gelatinized at 99 °C (30 min, 600 rpm), cooled, and modified by *Ro*BE (0.3 U/g starch) at 60 °C for 20 h (Li et al., 2019). The reaction was terminated by heating (99 °C, 30 min), followed by cooling to RT. The modified starch was treated using a sonicator (Q500, QSONICA, U.S.) at 400 W continuously for 10 min, a condition optimized to ensure effective aggregate disruption while maintaining structural integrity (Boufi et al., 2018), followed by centrifuged (20,000 *g*, 10 min). The three ss-sNPs (named WPS-NP, NPS-NP, and HPS-NP) were obtained in the supernatant, frozen O/N at −80 °C and freeze-dried for further analysis and use.

2.3. Size-exclusion chromatography (SEC)

The molecular weight distribution of the starch α-glucans was analyzed using a Size Exclusion Chromatography-Triple Detector Array (SEC-TDA) system equipped with a GRAM pre-column and GRAM1000 column connected to a TDA302 detection array (Viscotek, Malvern, UK). Differential refractive index (DRI) signals were recorded by an RI detector (PN3140, PostNova Analytics, Landsberg, Germany), and the data analyzed using PSS WinGPC Unity software (Polymer Standard Services, Mainz, Germany) (Tian et al., 2024). Starch samples (5 mg) dissolved in 1 mL DMSO/LiBr (0.5% *w*/w, 80 °C, O.N.) were injected onto the SEC system without prior filtration to prevent shear degradation (Cave, Seabrook, Gidley, & Gilbert, 2009) and eluted with DMSO/LiBr at 65 °C and a flow rate of 0.5 mL/min.

2.4. Chain length distribution (CLD)

For CLD analysis starch (5 mg/mL) was resuspended in 50 mM sodium acetate (pH 5.5), gelatinized (99 °C, 30 min), added pullulanase to a final concentration of 50 nM, incubated (40 °C, 3 h), and centrifuged (10,000 *g*, 5 min). Subsequently, 40 μL debranched starch solution was injected onto a CarboPac PA-200 column connected to a high performance anion exchange chromatography with pulsed amperometric detection (HPAEC-PAD) system (Dionex, Sunnyvale, CA, USA) and analyzed as previously described (Tian, Liu, et al., 2024).

2.5. ^{1}H NMR

One-dimensional (1D) proton (^{1}H) nuclear magnetic resonance (NMR) spectra of starch samples were acquired using a 600 MHz NMR spectrometer (Bruker Avance III, Bruker Biospin, Rheinstetten, Germany) (Xue, Wang, Li, & Bai, 2022). Starch (5 mg/mL) was suspended in D_2O, gelatinized (99 °C, 2 h), freeze-dried twice, and redissolved in D_2O (0.03% in TMSP, 99 °C, 30 min) before analysis. The degree of α-glucan branching was defined as moles α-1,6 glycosidic linkages divided by total moles of glycosidic linkages as estimated from the areas of signals representing anomeric protons (α-1,4-linkage: δ 5.35–5.45; α-1,6-linkage δ 4.95–5.00).

2.6. In vitro digestibility of ss-sNPs

Starch (20 mg) was suspended in 2 mL of 50 mM sodium acetate buffer containing 5 mM $CaCl_2$ (pH 5.5), and subsequently gelatinized (99 °C, 1 h, 1100 rpm). After cooling to 37 °C, the suspension was treated with 2 mg/mL pancreatin and 3.6 μM GA, followed by incubation at 37 °C under shaking at 300 rpm. Aliquots (50 μL) were collected at 0, 10, 20, 30, 40, 60, 90, 120, and 180 min, immediately mixed with 95% ethanol (500 μL), and centrifuged (10,000 *g*, 5 min). Glucose content in the supernatant was quantified using the GOPOD assay (D-Glucose Assay Kit, Megazyme, Wicklow, Ireland) and glucose as the standard (Huggett, 1957). Resistant starch (RS) was defined as the starch not hydrolyzed after 120 min. The dietary utilization of starch-based food materials is readily assessed by *in vitro* digestion monitoring contents of rapidly digested (RDS), slowly digested (SDS), and resistant starch (RS). The starch fractions were categorized based on the incubation time. Rapidly digestible starch (RDS) was defined as the starch hydrolyzed within 20 min; slowly digestible starch (SDS) was the starch hydrolyzed between 20 and 120 min; and resistant starch (RS) was the fraction remaining unhydrolyzed after 120 min (Englyst, Kingman, & Cummings, 1992; Zhang, Ao, & Hamaker, 2006). The contents of RDS, SDS, and RS were calculated according to equations Eqs. (1), (2), and (3), respectively,

$$\mathrm{RDS}(\%) = (\mathrm{G20} - \mathrm{FG})*0.9*100/\mathrm{TS} \quad (1)$$

$$\mathrm{SDS}(\%) = (\mathrm{G120} - \mathrm{G20})*0.9*100/\mathrm{TS} \quad (2)$$

$$\mathrm{RS}(\%) = (\mathrm{TS} - \mathrm{RDS} - \mathrm{SDS})*100/\mathrm{TS} \quad (3)$$

where TS is total starch content. FG represents the free glucose content (mg) in samples before hydrolysis, and G_{20} and G_{120} represent the glucose released within 20 and 120 min, respectively.

2.7. Dynamic light scattering (DLS)

The ss-sNPs (1%, *w/v*) were dispersed in Milli-Q water, and their particle size distribution, polydispersity index (PDI), and zeta potential were measured using a Zetasizer (Zetasizer Nano ZSP) at RT Size. Measurements were determined in triplicate (Chen, Ding, et al., 2024).

2.8. Storage stability of ss-sNPs

The dissolved ss-sNPs (1%, w/v in water) were stored at RT (25 °C) for 28 d to evaluate stability. Samples were withdrawn for particle size analysis as described in Section 2.7 at intervals of 1, 3, 7, 14, 21, and 28 d.

2.9. Scanning electron microscopy (SEM)

For morphological characterization, 20 μL of ss-sNPs (1%, w/v) was affixed onto aluminum SEM stubs, dried by evaporation (40 °C, 10 min) and coated with 6 nm of gold using a Leica EM ACE200 gold coater (Leica Microsystems, Wetzlar, Germany). The morphology of the ss-sNPs was observed using a field emission scanning electron microscope (FE-SEM) on an FEI Quanta 200 microscope at a magnification of 50,000×, following established protocols (Tian et al., 2023).

2.10. Fourier transform infrared-attenuated total reflectance (FTIR-ATR) spectroscopy

Starch samples were equilibrated to approx. 50% relative humidity prior to analysis using a Bomem MB100 FTIR spectrometer (ABB-Bomem, Quebec, Canada) equipped with a Golden gate attenuated total reflectance (ATR) accessory. Spectra for each sample were combined by co-adding at a resolution of 4 cm^{-1}, with a background spectrum collected through 128 co-added scans. Deconvolution was performed assuming a Lorentzian line shape with a half-width of 19 cm^{-1} and a resolution enhancement factor of 1.9 was assumed (Tian et al., 2024). Following baseline correction and deconvolution, IR absorbance values at 1022 and 1045 cm^{-1} were extracted from the spectra using OMNIC software (Capron, Robert, Colonna, Brogly, & Planchot, 2007).

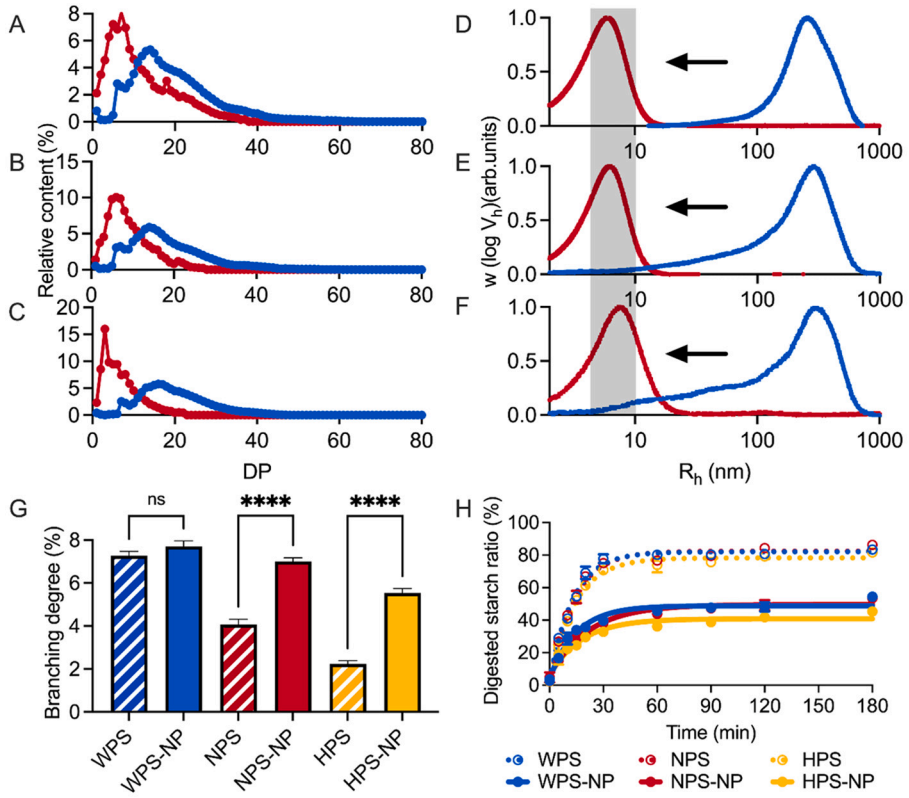

Fig. 1. Molecular structural analysis and *in vitro* digestibility of ss-sNPs and native starches. Chain length distribution (CLD) for (A) WPS, (B) NPS and (C) HPS. Molecular weight distribution for (D) WPS, (E) NPS and (F) HPS. (G) Degree of branching. (H) *In vitro digestibility*. *W(logV_h) represents molecular weight distribution based on the relationship. Between elution volume and hydrodynamic radius (logV_h) for pullulan standards. DP = degree of polymerization. Rh = hydrodynamic radius. **** represent statistical significance with p < 0.0001. The abbreviation 'ns' denotes non-significant differences.*

2.11. Wide-angle X-ray scattering (WAXS)

To analyze crystalline allomorphs and relative crystallinity, ss-sNPs were equilibrated at 90% relative humidity for 48 h prior to measurement. Analysis was performed using a Nano-inXider instrument (Xenocs SAS, Grenoble, France) with a 0.1542 nm wavelength Cu-Kα radiation (Wang et al., 2025). Radially averaged intensity (I) was plotted against scattering angle (2θ) of 5–40°. Relative crystallinity was quantified following established methods by using the PeakFit software (version 4.12) (Brückner, 2000).

2.12. Effect of ss-sNPs on in vitro digestion of granular wheat starch

Normal wheat starch (20 mg) was suspended 2 mL of buffer (50 mM sodium acetate, 5 mM $CaCl_2$, pH 5.5). The suspension was preheated (37 °C, 10 min), supplemented with 1 mg/mL ss-sNPs, and subsequently incubated with 2 mg/mL pancreatin and 3.6 μM GA under the conditions specified in Section 2.6 (37 °C, 3 h, 1100 rpm). Aliquots (50 μL) were collected for glucose analysis as in Section 2.6 (Huggett, 1957).

2.13. Interfacial kinetics analysis on granular wheat starch

Two complementary approaches, conventional and inverse Michaelis-Menten (MM) analyses, were employed to characterize the interfacial catalytic kinetics of granular wheat starch hydrolysis by GA. For conventional MM analysis, wheat starch granules (160 μL, 15–150 mg/mL) were pre-incubated (37 °C, 10 min, 1100 rpm) with varying concentrations of ss-sNPs (20 μL, 0, 0.5, 1, and 2 mg/mL). GA was added to a final concentration of 0.7 nM. For inverse MM analysis, starch granules (160 μL, 15 mg/mL) were treated with 20 μL ss-sNPs (0, 0.5, 1, and 2 mg/mL) and 20 μL GA (7 concentrations 0.7–171 nM). After 3 min reaction period, aliquots (100 μL) were transferred to new tubes, mixed with 20 μL 1.8 M Na_2CO_3 to stop the reaction, centrifuged (10,000 *g*, 5 min), and reducing sugar in the supernatant was quantified using the PAHBAH method (Lever, Powell, Killip, & Small, 1973).

Conventional MM data were analyzed using eq. 4 for non-linear regression analyses, S_0^{mass} being the substrate mass load, $K_{1/2}$ (in g × L^{-1}) the mass load at substrate half-saturation, and V_{max} (in M × s^{-1}) (Kari, Andersen, Borch, & Westh, 2017; Wang et al., 2025).

$$v_0 = \frac{V_{max} S_0^{mass}}{K_{1/2} + S_0^{mass}} \quad (4)$$

The inverse MM experiments were analyzed using eq. 5 by nonlinear regression analysis to give the parameters $^{inv}V_{max}$ (in g × L^{-1} × s^{-1}) and $^{inv}K_M$ (in M) being the enzyme concentration at half saturation.

$$v_0 = \frac{^{inv}V_{max} E_0}{^{inv}K_M + E_0} \quad (5)$$

The attack site density ($^{kin}\Gamma_{max}$) was calculated by eq. 6 using V_{max} (eq. 4) and $^{inv}V_{max}$ (eq. 5)(Kari et al., 2017).

$$\frac{\frac{^{inv}V_{max}}{S_0^{mass}}}{\frac{V_{max}}{E_0}} = {}^{kin}\Gamma_{max} \quad (6)$$

2.14. Langmuir adsorption on starch granules by GA

Wheat starch granules (160 μL, 20 mg/mL) were mixed with 20 μL ss-sNPs (0, 0.5, 1, and 2 mg/mL) and 20 μL GA was added to 7 final concentrations: 6.8–1400 nM, and the samples incubated (37 °C, 10 min, 1100 rpm), centrifuged (10,000 *g*, 5 min), and 100 μL supernatant was mixed with 100 μL 2.5-fold diluted Protein Assay Dye Reagent (Bio-Rad). Enzyme concentration was determined by measuring absorbance ratio at 590 nm and 450 nm, using Bovine Serum Albumin (BSA, Sigma)

Table 2
Branching parameters and *in vitro* digestibility of native starches and ss-sNPs.

Parameter (%)	WPS	WPS-NP	NPS	NPS-NP	HPS	HPS-NP
fa-chain[1]	25.0 ± 0.6^{d}	63.5 ± 0.9^{c}	26.1 ± 0.4^{d}	77.9 ± 0.9^{b}	16.9 ± 0.7^{e}	88.1 ± 0.5^{a}
fb_1-chain[1]	48.7 ± 0.3^{c}	28.5 ± 0.7^{d}	51.3 ± 0.7^{b}	21.3 ± 0.4^{e}	57.2 ± 0.5^{a}	11.9 ± 0.7^{f}
fb_2-chain[1]	17.7 ± 0.7^{a}	7.8 ± 0.4^{c}	15.4 ± 0.5^{b}	0.8 ± 0.5^{d}	20.6 ± 1.2^{a}	0.0 ± 0.9^{e}
fb_3-chain[1]	8.6 ± 0.2^{a}	0.2 ± 0.2^{d}	7.2 ± 0.3^{b}	0.0 ± 0.5^{d}	5.3 ± 0.4^{c}	0.0 ± 0.3^{d}
DP_{ave}	19.5 ± 0.5^{a}	11.6 ± 1.1^{b}	18.5 ± 0.4^{a}	9.0 ± 1.1^{c}	19.6 ± 0.9^{a}	6.2 ± 0.5^{d}
Degree of branching	7.3 ± 0.2^{a}	7.7 ± 0.3^{a}	4.1 ± 0.2^{c}	7.0 ± 0.3^{a}	2.2 ± 0.1^{d}	5.5 ± 0.1^{b}
RDS	69.1 ± 3.8^{a}	35.7 ± 0.8^{c}	66.9 ± 1.9^{a}	32.0 ± 1.1^{c}	61.3 ± 1.1^{b}	29.6 ± 0.4^{c}
SDS	19.4 ± 2.9^{a}	12.5 ± 2.0^{b}	17.4 ± 1.5^{a}	17.3 ± 1.1^{a}	17.8 ± 2.1^{a}	12.1 ± 0.7^{b}
RS	11.4 ± 0.0^{c}	51.8 ± 2.8^{a}	15.7 ± 0.4^{c}	50.7 ± 2.2 ^{a}	20.8 ± 1.0^{b}	58.2 ± 1.1^{a}

fa-chain: amylopectin (AP) chains with DP < 13, fb_1-chain: AP chains with DP 13–24, fb_2-chain: AP chains with DP 25–36, fb_3-chain: AP chains with DP > 36 (Bertoft, 2017).Values are expressed as mean ± standard deviation (n = 3). Different lower case superscript letters (a–f) within the same row indicate significant differences between samples (p < 0.05) based on one-way ANOVA test.

as standard. The data were analyzed using GraphPad Prism 6 (GraphPad Software Inc) and fitted to the *Langmuir* isotherm (eq. 7), where K_d represents the dissociation constant and $^{ads}\Gamma_{max}$ the (apparent) saturation coverage (Kari et al., 2017).

$$\Gamma = \frac{\Gamma_{ads\,max} * E_{free}}{K_d + E_{free}} \tag{7}$$

2.15. Langmuir adsorption by ss-sNPs to starch granules

Wheat starch granules (180 μL, 20 mg/mL) were mixed with 20 μL ss-sNP (7 final concentrations: 0.1–9 mg/mL), incubated (37 °C, 10 min, 1100 rpm), and centrifuged (10,000 *g*, 5 min). The concentration of ss-sNP in the colloidal suspension, indicated as the starch content, was quantified using the total starch assay (Total Starch Assay Kit (AA/AMG), Megazyme, Wicklow, Ireland). The data were analyzed using GraphPad Prism 6 (GraphPad Software Inc) and fitted the modified *Langmuir* isotherm (eq. 8), where Γ is the bound ss-sNPs, K_d the dissociation constant, and B_{max} the (apparent) saturation coverage (Kari et al., 2017).

$$\Gamma = \frac{B_{max} * [\text{Free ss} - \text{sNPs}]}{K_d + [\text{Free ss} - \text{sNPs}]} \tag{8}$$

2.16. Statistical analysis

All experiments were performed in triplicate. The statistical significance was assessed with one-way analysis of variance (ANOVA) using

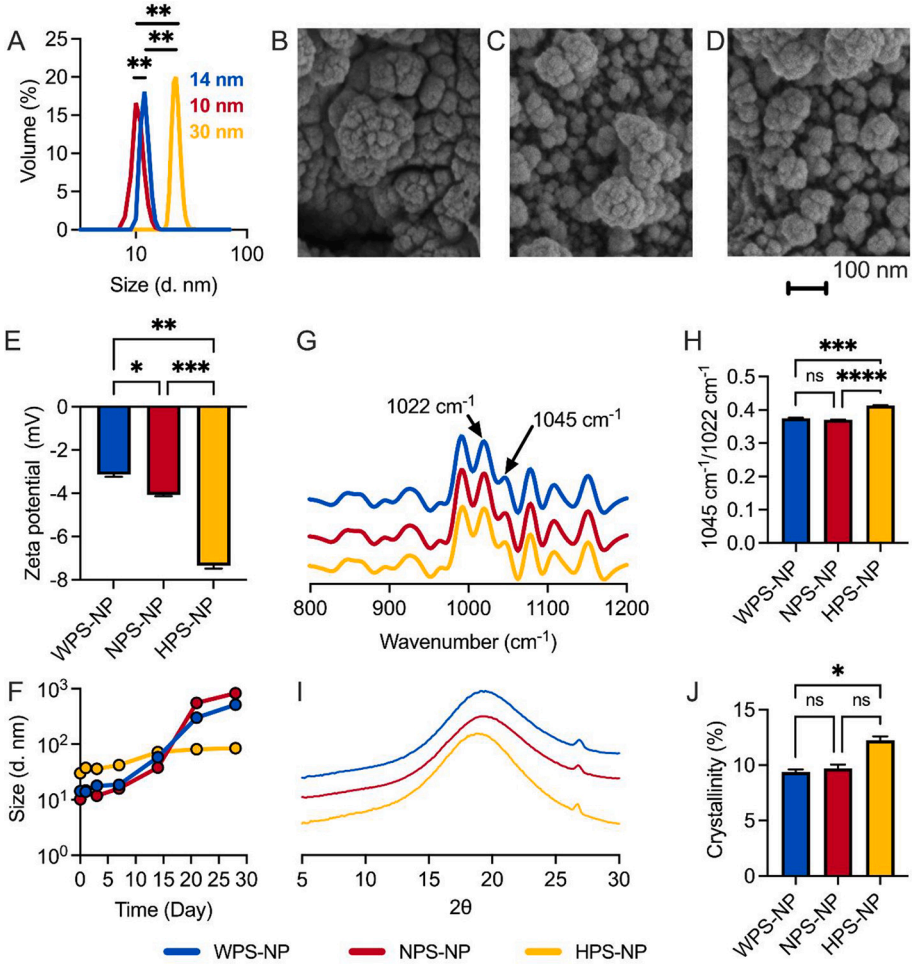

Fig. 2. Multi-level analysis of ss-sNPs. (A) Particle size distribution from zeta-sizer. Measurements. SEM image of (B) WPS-NP, (C) NPS-NP, and (D) HPS-NP. (E) Zeta potential. (F) Particle size of ss-sNPs during storage (0–28 d). (G) FTIR-ATR spectroscopy patterns and (H) degree of short-range order (1045 cm^{-1}/1022 cm^{-1}). (I) XRD patterns and (J) crystallinity. *, **, ***, and **** represent statistical significance with $p < 0.05$, $p < 0.01$, $p < 0.001$, and $p < 0.0001$. The abbreviation 'ns' denotes non-significant differences.

SPSS 20.0 (SPSS Inc., Chicago, USA). p-values <0.05 were considered statistically significant throughout the study.

3. Results and discussion

3.1. Molecular structure of native starches and ss-sNPs

Analysis of the chain length distribution (CLD) revealed significant changes in the distribution of fa (degree of polymerization, DP 6–12), fb1 (DP 13–24), fb2 (DP 25–36), and fb3 (DP > 36) chain fractions (Bertoft, 2017; Bertoft, Blennow, & Hamaker, 2024). Specifically, WPS-NP exhibited a 2.5-fold increase in fa alongside 1.7- and 2.3-fold decreases in fb_1 and fb_2 chains, respectively and this trend was consistent across NPS and HPS (Fig. 1A–C, Table 2). Notably, HPS-NP possessed the shortest chains, average DP (DP_{ave}) 1.9, 1.5-fold lower than the WPS-NP and NPS-NP (Table 2). Mechanistically, *Ro*BE catalyzes the cleavage of α-1,4-glycosidic linkages in long amylopectin chains (fb_2, fb_3) and transfers the cleaved off moieties to form new branch points, thereby increasing the population of short linear chains. Furthermore, the subsequent ultrasonication induces high-intensity acoustic cavitation that preferentially degrades the macromolecular chains into lower molecular weight fragments, and shorter chain length. The pronounced reduction in HPS-NP suggests that the specific structural arrangement of HPS may be more susceptible to this dual-modification induced degradation.

SEC analysis of the molecular size of the native (not debranched) starches distinguished two regions: amylopectin (molecular hydrodynamic radius, R_h > 66 nm) and amylose ($R_h \leq 66$ nm). In contrast, all ss-sNPs exhibited single peaks at molecular R_h < 10 nm. Specifically, the molecular size was slightly higher for HPS-NP compared to WPS-NP and NPS-NP (Fig. 1D–F) (Tian, Liu, et al., 2024; Vilaplana & Gilbert, 2010). This confirms that the constituent polymer chains of the NPs have been significantly degraded compared to the native starch molecular structure. The degree of branching determined by ^{1}H NMR analysis indicated minor change for WPS-NP, but revealed 1.7- and 2.5-fold increase, respectively, for NPS-NP and HPS-NP compared to the native starches (Fig. 1G, Table 2). The higher fold-increase for HPS-NP demonstrates the efficacy of *Ro*BE in catalyzing the transfer of new branch chains. The findings align with our previous study, where *Ro*BE is suggested to act preferentially on amylose, making NPS and HPS superior substrates as WPS contains very little amylose (Chen, Wang, et al., 2024). These results confirmed that the ss-sNPs being uniform starch particles with R_h < 10 nm are highly branched and carry shorter branch chains than the native starches. In HPS-NP, the combination of lower DP_{ave}, lower degree of branching and slightly higher R_h than in WPS-NP and NPS-NP, indicated that HPS-NP maintained a part of free linear segments (Fig. 1A–F, Table 2).

Regarding digestibility profiles, the gelatinized native WPS exhibited the highest RDS content among the three samples. This is attributed to its greater branching density and consequently higher frequency of non-reducing ends, which serve as primary substrates for GA used as a gut glucosidase mimic. As anticipated, *Ro*BE modification significantly reduced the RDS and increased RS in all three ss-sNPs compared to the corresponding native starches. The introduced new branching points in starch (Wang et al., 2024), disfavored degradation by α-amylase conferring the ss-sNPs with potential health promoting assets and tailored digestibility for controlled delivery of substances.

3.2. Structure and mechanism of formation of ss-sNPs

Having established that the enzymatic and ultrasonic treatments successfully generated highly branched, short-chain glucans (Section 3.1), we further investigated how these molecular characteristics translate into the physical and colloidal properties of the assembled ss-sNPs. The ss-sNPs exhibited a hydrodynamic radii (R_h) of 10–30 nm and a narrow size distribution (PDI < 0.3, data not shown) determined by molecular weight distribution (Fig. 1D–F), known to be appropriate for ss-sNPs (Chen, Wang, et al., 2024). It is important to note the distinction between the molecular R_h (<10 nm) obtained *via* SEC, which reflects the size of individual dissolved chains, and the hydrodynamic diameter (D_h) (10–30 nm) obtained *via* DLS, which represents the diameter of the hydrated nanoparticle assembly in suspension. The NPS-NP at 10.2 ± 0.1 nm was the smallest, followed by WPS-NP at 14.3 ± 0.1 nm, and HPS-NP at 30.0 ± 0.7 nm (Fig. 2A, Table 3). In a previous study, low yields of ss-sNPs (<10%) were obtained by extracting branched starches with R_h = 10–20 nm from high-amylose maize starch by nano-precipitation using ethanol (Chen, Ding, et al., 2024). The yield of the three ss-sNPs originating from *Ro*BE treatment in this study (Table 3) was considerably higher, confirming that the highly branched starches with R_h < 10 nm are suitable for preparing ss-sNPs. Furthermore, it has been demonstrated that debranched short chain-length starch leads to larger sNPs, while debranched long chain-length starch yields sNPs of smaller size (Duyen, Phi, & Van Hung, 2022).

Table 3
Yield, particle size, zeta potential, 1045 cm^{-1}/1022 cm^{-1} value, and crystallinity of the ss-sNPs.

Parameter	WPS-NP	NPS-NP	HPS-NP
Yield (%)	88.5 ± 0.8[1,2,b]	92.7 ± 1.3[a]	93.1 ± 0.9[a]
Particle size (nm)	10.2 ± 0.1[c]	14.3 ± 0.1[b]	30.0 ± 0.7[a]
Zeta potential (mV)	−7.1 ± 0.1[a]	−7.3 ± 0.1[a]	−3.1 ± 0.1[b]
1045 cm^{-1}/1022 cm^{-1}	0.38 ± 0.003[a]	0.37 ± 0.006[a]	0.41 ± 0.007[a]
Crystallinity (%)	9.4 ± 0.3[b]	9.7 ± 0.5[b]	12.2 ± 0.5[a]

[1] Means ± standard deviation.
[2] Different letters in the same row indicate significant differences at $p < 0.05$.

The morphological analysis of the NP preparations *via* SEM (Fig. 2B–D) revealed significant aggregation of the ss-sNPs, with no distinct individual NPs observable after solvent evaporation. Such aggregation is typically found for NPs and due to the large surface area of the NPs exposing a high number of hydroxyl groups facilitating strong hydrogen bonding, leading to particle clustering (Du et al., 2023; Mohammad Amini & Razavi, 2016). Previous data on NP aggregation demonstrate that a high absolute zeta potential enhances electrostatic repulsion, thereby reducing the Van der Waals forces of attraction responsible for particle agglomeration, hence preventing formation of aggregates (Ahmad, Gani, Hassan, Huang, & Shabbir, 2020; Schäfer, Hecht, Harting, & Nirschl, 2010). Consequently, the larger particle size of HPS-NP might stem from its 2.3–2.4-fold smaller negative zeta-potential than of WPS-NP and NPS-NP (Fig. 2E, Table 3). The D_h of the ss-sNPs was monitored over 28 d of storage (Fig. 2F). The size of WPS-NP and NPS-NP remained virtually stable for 7 d, before increasing notably from 18.5 to 516 nm and 16.0 to 833 nm, respectively, between day 8 and 28. However, the size of HPS-NP only increased 2.8-fold from 30 to 84 nm after 28 d (Fig. 2F). This superior long-term stability of HPS-NP not only to stronger electrostatic repulsion but also to its internal structure, characterized by a more densely packed glucan matrix that imparts greater structural rigidity. This compact configuration likely restricts water uptake and limits the swelling-induced expansion of the polymer network that was more pronounced in the more loosely organized WPS and NPS matrices. The pronounced instability in WPS-NP and NPS-NP suggests limitations for their use in long-term aqueous application, potentially requiring lyophilization for storage. In contrast, the relative structural persistence of HPS-NP facilitates its application in liquid-based functional foods or Pickering emulsions where long-term colloidal stability is critical.

The ratio of the FTIR-ATR intensities at 1045 and 1022 cm^{-1} describes the short-range order of starch (Yaskin Harush, Shani Levi, & Lesmes, 2025). The 1045 cm^{-1}/1022 cm^{-1} value of HPS-NP (0.41) was higher than of WPS-NP (0.38) and NPS-NP (0.37) (Fig. 2G, H, Table 3). HPS-NP also possessed higher long-range order (crystallinity) than WPS-NP and NPS-NP as assessed by WAXS (Fig. 2I, J, Table 3). Similar highly amorphous characteristics and diminished crystalline regions of ss-sNPs (Fig. 2I) has been previously observed for starch-based NPs (Ahmad

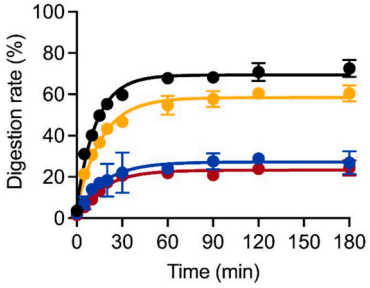

Fig. 3. Effect of addition of ss-sNPs on *in vitro* digestion of granular wheat starch by α-amylase in pancreatin and GA, serving as intestinal disaccharidase mimic. Black: without ss-sNP, blue: with WPS-NP, red: with NPS-NP, and yellow: with HPS-NP. (For interpretation of the references to colour in this figure legend, the reader is referred to the web version of this article.)

et al., 2020, 2019).

The formation of sNPs involves a notable molecular re-organization, establishing double helical segments between α-glucan chains (Le Corre et al., 2010). The fewer branching points and shorter amylopectin chains found in HPS-NP (Fig. 1G, Table 2), suggests a trend for enabling the formation of molecularly ordered products during ss-sNPs fabrication. Hence, HPS-NP had ordered structure, possibly helices, in turn arranged an ordered crystalline section (high crystallinity) compared to WPS-NP and NPS-NP containing more branching points and longer branches (Fig. 2A–C, Table 2). As a result, higher size stability after 28 d in HPS-NP (Fig. 2F) likely stems from its more ordered structure (Fig. 2G–J).

3.3. *In vitro digestion and applying interfacial kinetics to describe the inhibition by ss-sNPs of enzymatic hydrolysis of granular starch*

The distinct structural and physicochemical properties of WPS-NP, NPS-NP, and HPS-NP prompted us to investigate their functional performance as inhibitors of interfacial starch digestion. Granular starch is classified as type 2 resistant starch (RS2), which is gaining recognition for its nutritional benefits in suppressing glycemic levels and mitigating related lifestyle-associated health risks (Tian, Wang, Zhong, et al., 2023). Previous studies established that sNPs effectively inhibit starch hydrolases, such as α-amylase, hence reducing digestion (Jiang et al., 2018; Yang et al., 2025). Among the present ss-sNPs, the antiglycemic potential was highest of NPS-NP and WPS-NP, while HPS-NP had only a minor effect as analyzed by *in vitro* digestion of granular wheat starch by GA and pancreatin (Fig. 3).

The inhibitory effects were further analyzed using an interfacial kinetics approach and *Langmuir* adsorption isotherms (Table 4, Fig. 4–6). Varying the concentrations of WPS-NP and NPS-NP using conventional Michaelis–Menten (MM)-kinetics (Fig. 4A, B), the fitted double reciprocal plots of the initial velocity *vs* substrate concentration, intersected the X-axis at the same point, indicating noncompetitive inhibition (Fig. 4G, H). By contrast, the double reciprocal plots for HPS-NP yielded parallel lines, signifying uncompetitive inhibition (Fig. 4I) (Jiang et al., 2018). The interfacial kinetics and the *Langmuir* adsorption isotherm analyses returned the densities of attack sites ($^{kin}\Gamma_{max}$), respectively binding sites ($^{abs}\Gamma_{max}$) on the substrate (Table 2) (Wang et al., 2025). Notably, clear negative correlation was found between the ss-sNPs concentration and $^{kin}\Gamma_{max}$ and $^{abs}\Gamma_{max}$ (Fig. 6A, B). Thus, WPS-NP and NPS-NP strongly weakened the ability of GA to recognize attack and binding sites on the wheat starch granules. Furthermore, the dissociation constant (K_d) increased from 127 nM in the control (without ss-sNPs) to 237 nM (WPS-NP) and 158 nM (NPS-NP) at the highest inhibitor concentration. In the *Langmuir* adsorption isotherm, increased K_d indicates reduced binding affinity. In our complex ternary system, this shift likely reflects not just a change in individual site affinity, but also a competitive interaction between ss-sNPs and GA for the same interfacial area. The inhibitory mechanism likely more involved, as opposed to HPS-NP, WPS-NP and NPS-NP interacting effectively with the GA active site, and with the substrate granule independently, due to their small size and large surface area (Fig. 2A) as well as less ordered structure (Figs. 2H, J and 7).

The observed size-dependent effect of ss-sNPs reflects fundamental differences in interactions among the NPs, starch granule substrates, and degrading enzymes. WPS-NP and NPS-NP of 10–14 nm (Fig. 2A) have larger relative surface area than HPS-NP of 30 nm, and potentially bind more GA (~6 nm) (Sankaran, Sivakami, Radhakrishnan, & Pandit, 1983), which effectively reduces its availability to the starch granules. Importantly, the size of WPS-NP and NPS-NP is optimal for blocking the surface pores on wheat starch granules, ranging from10.7 to 12 nm, reported to be efficient enzyme attack sites (Fig. 8B) (Wu, Zhang, Ma, Sui, & Corke, 2026; Zhang et al., 2023). In addition, GA possibly showed lower binding to the larger HPS-NP, 30 nm, which would be excluded from the granule pores thereby having less influence on hydrolysis by

Table 4
Interfacial kinetics and *Langmuir* adsorption parameters for GA degrading granular wheat starch and inhibited by added ss-sNPs.

Type of ss-sNPs	[ss-sNPs] (mg/mL)	k_{cat}[1] (s^{-1})	$K_{1/2}$[2] ($g{\cdot}L^{-1}$)	$^{inv}k_{cat}$[3] ($nmol{\cdot}g^{-1}{\cdot}s^{-1}$)	$^{kin}\Gamma_{max}$[4] (nmol/g)	$^{abs}\Gamma_{max}$[5] (nmol/g)	A/B ratio[6] (%)	K_d[7] (nM)
WPS-NP	0	52.3 ± 4.6[8,9,a]	44.7 ± 5.5[b]	357 ± 38[a]	6.6 ± 0.7[a]	10.5 ± 1.1[a]	62.9 ± 0.1[b]	127 ± 11[a]
	0.5	42.3 ± 3.3[b]	52.9 ± 6.9[ab]	270 ± 41[b]	6.4 ± 0.4[a]	8.5 ± 0.7[b]	75.3 ± 1.2[a]	270 ± 16[a]
	1	40.0 ± 5.1[bc]	59.6 ± 8.3[a]	201 ± 44[c]	5.0 ± 0.5[b]	6.7 ± 0.4[c]	74.6 ± 2.5[a]	87 ± 12[a]
	2	33.7 ± 2.2[c]	51.7 ± 5.9[ab]	128 ± 16[d]	3.8 ± 0.3[c]	6.0 ± 0.5[c]	63.3 ± 0.3[b]	237 ± 19[a]
NPS-NP	0	52.3 ± 4.6[a]	44.7 ± 5.5[a]	357 ± 38[a]	6.6 ± 0.7[a]	10.5 ± 1.1[a]	62.9 ± 0.1[c]	127 ± 11[ab]
	0.5	40.5 ± 2.9[b]	48.6 ± 6.3[a]	255 ± 21[b]	6.3 ± 0.3[ab]	7.3 ± 0.7[b]	86.3 ± 3.4[b]	141 ± 12[b]
	1	34.9 ± 3.8[bc]	45.4 ± 7.1[a]	189 ± 19[c]	5.4 ± 0.5[b]	6.0 ± 0.5[b]	90.0 ± 0.7[ab]	143 ± 16[a]
	2	29.9 ± 3.7[c]	39.6 ± 4.3[a]	121 ± 21[d]	3.8 ± 0.5[c]	4.0 ± 0.2[c]	95.0 ± 6.3[a]	158 ± 27[a]
HPS-NP	0	52.3 ± 4.6[a]	44.7 ± 5.5[a]	357 ± 38[a]	6.6 ± 0.7[a]	10.5 ± 1.1[a]	62.9 ± 0.1[c]	127 ± 11[ab]
	0.5	37.8 ± 2.5[b]	37.7 ± 5.2[a]	259 ± 24[b]	6.9 ± 0.8[a]	9.4 ± 0.3[ab]	73.4 ± 5.0[b]	99 ± 18[b]
	1	28.6 ± 1.9[c]	26.5 ± 5.8[b]	197 ± 37[bc]	6.9 ± 0.7[a]	8.9 ± 0.6[b]	77.5 ± 2.2[ab]	145 ± 21[a]
	2	24.3 ± 1.3[c]	22.5 ± 2.9[b]	144 ± 38[d]	5.9 ± 0.4[a]	8.4 ± 0.5[b]	70.2 ± 0.5[a]	148 ± 20[a]

[1] k_{cat}: turnover number from conventional MM-kinetics.
[2] $K_{1/2}$: mass load at substrate half-saturation from conventional MM-kinetics.
[3] $^{inv}k_{cat}$: turnover number from inverse MM-kinetics.
[4] $^{kin}\Gamma_{max}$: density of attack sites.
[5] $^{ads}\Gamma_{max}$: density of binding sites.
[6] A/B ratio: attack site density/binding site density ratio (percentage).
[7] K_d: binding constant.
[8] Values are means ± standard deviation.
[9] Different letters in the same row indicate significant differences at $p < 0.05$.

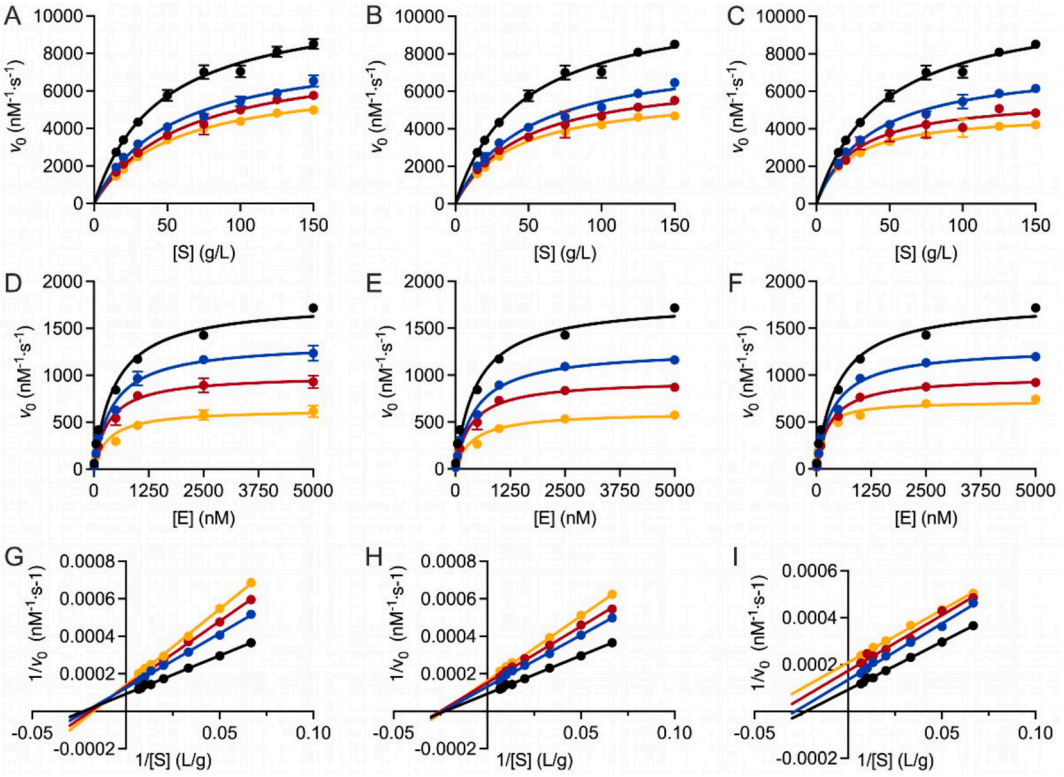

Fig. 4. Interfacial kinetics for GA hydrolysis of wheat starch granules in the presence of ss-sNPs at three different concentrations. Conventional MM-kinetics, effect of (A) WPS-NP, (B) NPS-NP, and (C) HPS-NP. Inverse MM-kinetics, effect of (D) WPS-NP, (E) NPS-NP, and (F) HPS-NP. Lineweaver-Burk plots based on conventional MM-kinetics with addition of (G) WPS-NP, (H) NPS-NP, and (I) HPS-NP. Black: 0 mg/mL, blue: 0.5 mg/mL, red: 1 mg/mL, and yellow: 2 mg/mL ss-sNPs. (For interpretation of the references to colour in this figure legend, the reader is referred to the web version of this article.)

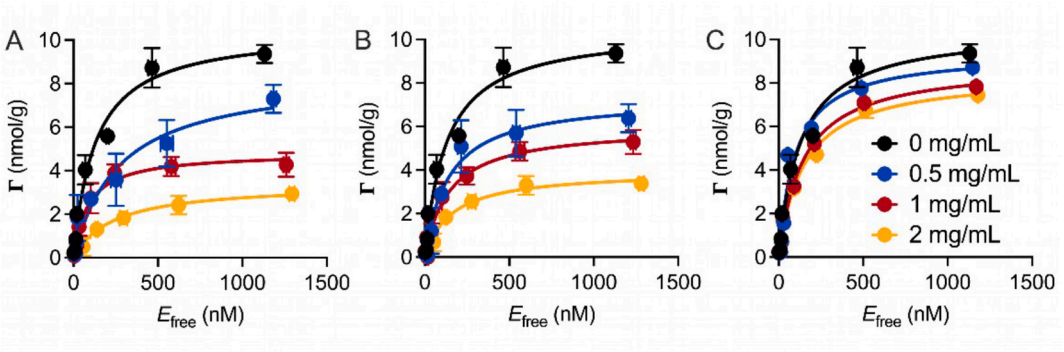

Fig. 5. *Langmuir* adsorption of GA on wheat starch granules in presence of ss-sNPs at three different concentrations. (A) WPS-NP, (B) NPS-NP, and (C) HPS-NP.

GA that can freely enter the pores (Fig. 8C). Furthermore, the GA binds less efficiently to these sNPs (Fig. 7). We therefore suggest that, besides the conventional inhibition modes, where an inhibitor interacts with the enzyme or enzyme–substrate complexes (Dixon, 1953; Li, Bai, Jin, & Svensson, 2022), ss-sNPs exert an inhibitory effect by also interacting with the substrate during interfacial enzyme catalysis (Fig. 8B,C). For example, the inhibitor primarily interacts with the pre-formed enzyme-substrate complex on the granule surface rather than blocking initial enzyme access. This size-dependent differentiation provides a kinetic rationale for the varying degrees of antiglycemic potential observed among the ss-sNPs (Fig. 3).

4. Conclusion

ss-sNPs were produced in a high yield of ~90% using an environmentally friendly approach involving combined enzymatic and sonication treatments. Three potato starch types (WPS, NPS, and HPS) with different amylose contents were modified by *Ro*BE followed by sonication, leading to ss-sNPs exhibiting distinct narrow particle size distributions (PDI < 0.3) in the 10–30 nm range. The three ss-sNPs showed high stability for approximately a week, which is relevant for most practical applications. Furthermore, the ss-sNPs were distinctly more resistant in *in vitro* digestibility tests than the native starches, attributed to the higher branch chain contents. Notably, the ss-sNPs inhibited hydrolysis of wheat starch granules by GA due to fewer available attack sites as measured using an interfacial kinetics analysis approach. The smaller nanoparticles (10–14 nm), acting as noncompetitive inhibitors, presumably binding to GA and blocking the granular surface pores susceptible to GA on wheat starch granules. Conversely, the larger NPs (30 nm) did not occlude the pores and acted as weaker uncompetitive inhibitors. These results underscore the key role of size and branching structure of NPs in modulating enzymatic interactions

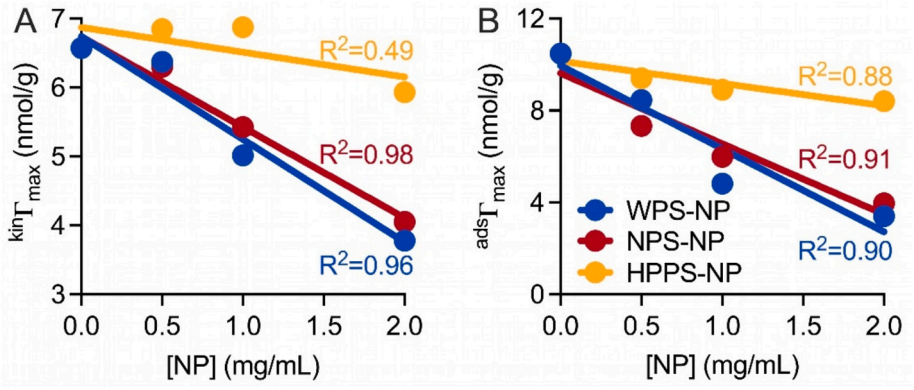

Fig. 6. Correlation analysis between ss-sNPs and GA (A) density of attack sites ($^{kin}\Gamma_{max}$) and (B) density of binding sites ($^{ads}\Gamma_{max}$).

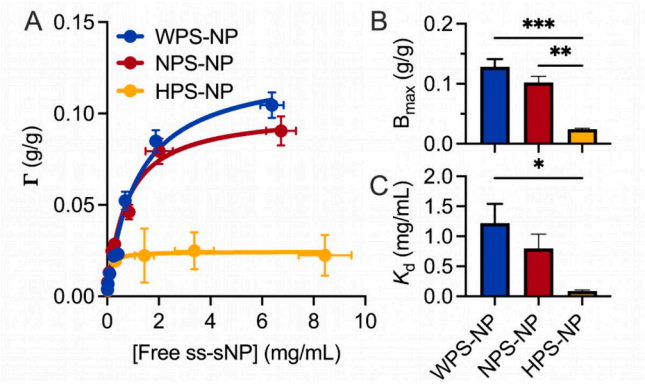

Fig. 7. *Langmuir* adsorption for ss-sNPs on wheat starch granules. (A) Binding isotherms. Lines represent best fits of the modified *Langmuir* equation (eq. 5; Section 2.15). (B) B_{max} (eq. 5). (C) K_d. *, **, and *** represent statistical significance with $p < 0.05$, $p < 0.01$, and $p < 0.001$.

with substrates. Despite these promising results, challenges regarding long-term storage persist for some samples. In particular, the poor stability of WPS-NP and NPS-NP may constrain their shelf-life in commercial applications, although HPS-NP demonstrates superior stability. This difference underscores the need for a deeper understanding of particle interactions. Furthermore, while the interfacial kinetics model provides a robust theoretical framework, the precise molecular binding sites between GA and ss-sNPs have not been visually confirmed. Future studies employing advanced microscopy or molecular docking simulations are required to reduce this mechanistic uncertainty. Additionally, while these NPs show potential for regulating starch digestion, their physiological impact and safety within a complex food matrix or *in vivo* environment warrant further investigation. Future research should further explore the full scalability of this sonication-assisted process for industrial-scale production and evaluate the bio-functional performance of these NPs in diverse delivery systems for nutrition and biomedicine.

CRediT authorship contribution statement

Zhihang Li: Writing – original draft, Investigation, Data curation. **Yu Tian:** Writing – original draft, Investigation, Funding acquisition, Data curation. **Jacob Judas Kain Kirkensgaard:** Methodology. **Birte Svensson:** Writing – review & editing, Supervision, Funding acquisition, Conceptualization. **Andreas Blennow:** Writing – review & editing,

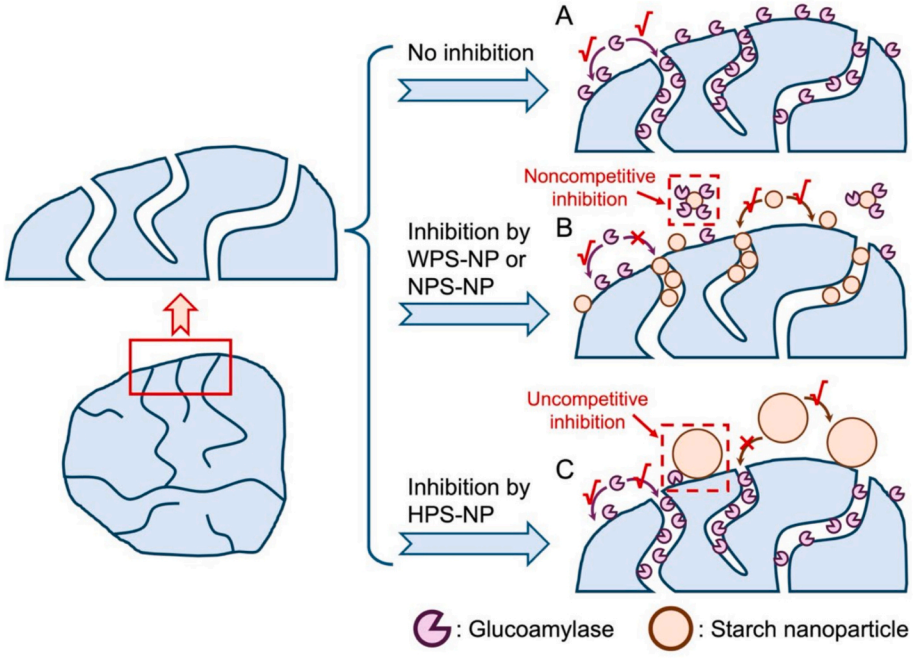

Fig. 8. Schematic view of catalytic activity of GA on wheat starch granules without ss-sNPs (A), in the presence of WPS-NP or NPS-NP (B) and of HPS-NP (C).

Supervision, Funding acquisition, Conceptualization. **Yu Wang:** Writing – review & editing, Supervision, Conceptualization.

Declaration of competing interest

The authors declare that they have no known competing financial interests or personal relationships that could have appeared to influence the work reported in this paper.

Acknowledgements

This work is supported by the Independent Research Fund Denmark, project BioMarch, grant #3105-00327B (BS and AB), ZL's personal funds (University of Copenhagen, #5441016), the China Postdoctoral Science Foundation #2025M772998 (YT), the Jiangsu Funding Program for Excellent Postdoctoral Talent #2025ZB30 (YT). Data were generated by accessing research infrastructure of the University of Copenhagen, including FOODHAY (Food and Health Open Innovation Laboratory, Danish Roadmap for Research Infrastructure). The authors thank Bekzod Khakimov (University of Copenhagen) for his technical assistance with ^{1}H NMR analysis. We also appreciate the constructive comments from Yitan Zhai (Wageningen University), Xingxun Liu (Nanjing University of Finance and Economics), as well as Yongxian Chen, Bodil Jørgensen, and Peter Ulvskov (University of Copenhagen).

Data availability

Data will be made available on request.

References

Ahmad, M., Gani, A., Hassan, I., Huang, Q., & Shabbir, H. (2020). Production and characterization of starch nanoparticles by mild alkali hydrolysis and ultrasonication process. *Scientific Reports, 10*(1), 1–11. https://doi.org/10.1038/s41598-020-60380-0

Ahmad, M., Mudgil, P., Gani, A., Hamed, F., Masoodi, F. A., & Maqsood, S. (2019). Nano-encapsulation of catechin in starch nanoparticles: Characterization, release behavior and bioactivity retention during simulated in-vitro digestion. *Food Chemistry, 270* (July 2018), 95–104. https://doi.org/10.1016/j.foodchem.2018.07.024

Balan, K., Qing, W., Wang, Y., Liu, X., Palvannan, T., Wang, Y., Ma, F., & Zhang, Y. (2016). Antidiabetic activity of silver nanoparticles from green synthesis using Lonicera japonica leaf extract. *RSC Advances, 6*(46), 40162–40168.

Bertoft, E. (2017). Understanding starch structure: Recent progress. *Agronomy, 7*(3), Article 56. https://doi.org/10.3390/AGRONOMY7030056

Bertoft, E., Blennow, A., & Hamaker, B. R. (2024). Perspectives on starch structure, function, and synthesis in relation to the backbone model of amylopectin. *Biomacromolecules, 25*(9), 5389–5401. https://doi.org/10.1021/acs.biomac.4c00369

Blennow, A., Wischmann, B., Houborg, K., Ahmt, T., Jørgensen, K., Engelsen, S. B., … Poulsen, P. (2005). Structure function relationships of transgenic starches with engineered phosphate substitution and starch branching. *International Journal of Biological Macromolecules, 36*(3), 159–168. https://doi.org/10.1016/j.ijbiomac.2005.05.006

Boufi, S., Bel Haaj, S., Magnin, A., Pignon, F., Impéror-Clerc, M., & Mortha, G. (2018). Ultrasonic assisted production of starch nanoparticles: Structural characterization and mechanism of disintegration. *Ultrasonics Sonochemistry, 41*(September 2017), 327–336. https://doi.org/10.1016/j.ultsonch.2017.09.033

Brückner, S. (2000). Pulwin: A program for analyzing powder X-ray diffraction patterns. *Powder Diffraction, 15*(4), 218–219. https://doi.org/10.1017/S0885715600011118

Campelo, P. H., Sant'Ana, A. S., & Clerici, M. T. P. S. (2020). Starch nanoparticles: Production methods, structure, and properties for food applications. *Current Opinion in Food Science, 33*, 136–140.

Capron, I., Robert, P., Colonna, P., Brogly, M., & Planchot, V. (2007). Starch in rubbery and glassy states by FTIR spectroscopy. *Carbohydrate Polymers, 68*(2), 249–259. https://doi.org/10.1016/j.carbpol.2006.12.015

Cave, R. A., Seabrook, S. A., Gidley, M. J., & Gilbert, R. G. (2009). Characterization of starch by size-exclusion chromatography: The limitations imposed by shear scission. *Biomacromolecules, 10*(8), 2245–2253.

Chen, Y., Ding, L., Di, H., Kirkensgaard, J. J. K., Sun, B., Pang, C., … Blennow, A. (2024). Green preparation of small-sized starch nanoparticles using nanoprecipitation. *Food Hydrocolloids, 153*, Article 109974. https://doi.org/10.1016/j.foodhyd.2024.109974

Chen, Y., Jiang, S., Wang, Y., Zhang, F., Wang, L., Zhao, L., … Blennow, A. (2024). Small-sized starch nanoparticles for efficient penetration of plant cells. *Chemical Communications, 60*, 14113–14116. https://doi.org/10.1039/d4cc05493h

Chen, Y., Wang, Y., Tian, Y., Svensson, B., & Blennow, A. (2024). Enzymatic synthesis of long-branched or short-branched starches with uniform molecular size. *Food Bioscience.* , Article 105353. https://doi.org/10.1016/j.fbio.2024.105353

Da Costa, D., Exbrayat-Héritier, C., Rambaud, B., Megy, S., Terreux, R., Verrier, B., & Primard, C. (2021). Surface charge modulation of rifampicin-loaded PLA nanoparticles to improve antibiotic delivery in *Staphylococcus* aureus biofilms. *Journal of Nanobiotechnology, 19*, 1–17.

Damager, I., Engelsen, S. B., Blennow, A., Lindberg Møller, B., & Motawia, M. S. (2010). First principles insight into the α-glucan structures of starch: Their synthesis, conformation, and hydration. *Chemical Reviews, 110*(4), 2049–2080. https://doi.org/10.1021/CR900227T

Deeksha, B., Sadanand, V., Hariram, N., & Rajulu, A. V. (2021). Preparation and properties of cellulose nanocomposite fabrics with in situ generated silver nanoparticles by bioreduction method. *Journal of Bioresources and Bioproducts, 6*(1), 75–81.

Dixon, M. (1953). The determination of enzyme inhibitor constants. *Biochemical Journal, 55*(1), 170.

Du, C., Jiang, F., Hu, W., Ge, W., Yu, X., & Du, S. (2023). Comparison of properties and application of starch nanoparticles optimized prepared from different crystalline starches. *International Journal of Biological Macromolecules, 235*(January), Article 123735. https://doi.org/10.1016/j.ijbiomac.2023.123735

Duyen, T. T. M., Phi, N. T. L., & Van Hung, P. (2022). Comparison in morphology, structure and functionality of curcumin-loaded starch nanoparticles fabricated from short, medium and long chain-length debranched cassava starches. *International Journal of Food Science and Technology, 57*(11), 6913–6924. https://doi.org/10.1111/ijfs.15389

Englyst, H. N., Kingman, S. M., & Cummings, J. H. (1992). Classification and measurement of nutritionally important starch fractions. *European Journal of Clinical Nutrition, 46*, S33–S50.

Erathodiyil, N., & Ying, J. Y. (2011). Functionalization of inorganic nanoparticles for bioimaging applications. *Accounts of Chemical Research, 44*(10), 925–935.

Fahimirad, S., Abtahi, H., Satei, P., Ghaznavi-Rad, E., Moslehi, M., & Ganji, A. (2021). Wound healing performance of PCL/chitosan based electrospun nanofiber electrosprayed with curcumin loaded chitosan nanoparticles. *Carbohydrate Polymers, 259*, Article 117640.

Flores, A. M., Ye, J., Jarr, K.-U., Hosseini-Nassab, N., Smith, B. R., & Leeper, N. J. (2019). Nanoparticle therapy for vascular diseases. *Arteriosclerosis, Thrombosis, and Vascular Biology, 39*(4), 635–646.

Goh, E. J., Kim, K. S., Kim, Y. R., Jung, H. S., Beack, S., Kong, W. H., … Hahn, S. K. (2012). Bioimaging of hyaluronic acid derivatives using nanosized carbon dots. *Biomacromolecules, 13*(8), 2554–2561.

Hamadani, C. M., Dasanayake, G. S., Gorniak, M. E., Pride, M. C., Monroe, W., Chism, C. M., … Edgecomb, S. X. (2023). Development of ionic liquid-coated PLGA nanoparticles for applications in intravenous drug delivery. *Nature Protocols, 18*(8), 2509–2557.

Hu, Q., Lu, Y., & Luo, Y. (2021). Recent advances in dextran-based drug delivery systems: From fabrication strategies to applications. *Carbohydrate Polymers, 264*, Article 117999.

Huggett, A. (1957). Enzymic determination of blood glucose. *The Biochemical Journal, 66*, 12P.

Jiang, S., Li, M., Chang, R., Xiong, L., & Sun, Q. (2018). *In vitro* inhibition of pancreatic α-amylase by spherical and polygonal starch nanoparticles. *Food & Function, 9*(1), 355–363. https://doi.org/10.1039/c7fo01381g

Kari, J., Andersen, M., Borch, K., & Westh, P. (2017). An inverse Michaelis-Menten approach for interfacial enzyme kinetics. *ACS Catalysis, 7*(7), 4904–4914. https://doi.org/10.1021/ACSCATAL.7B00838

Kou, T., Faisal, M., Song, J., & Blennow, A. (2023). Stabilization of emulsions by high-amylose-based 3D nanosystem. *Food Hydrocolloids, 135*, Article 108171.

Kozlov, S. S., Blennow, A., Krivandin, A. V., & Yuryev, V. P. (2007). Structural and thermodynamic properties of starches extracted from GBSS and GWD suppressed potato lines. *International Journal of Biological Macromolecules, 40*(5), 449–460. https://doi.org/10.1016/j.ijbiomac.2006.11.001

Le Corre, D., Bras, J., & Dufresne, A. (2010). Starch nanoparticles: A review. *Biomacromolecules, 11*(5), 1139–1153. https://doi.org/10.1021/bm901428y

Lever, M., Powell, J. C., Killip, M., & Small, C. W. (1973). A comparison of 4-hydroxybenzoic acid hydrazide (PAHBAH) with other reagents for the determination of glucose. *The Journal of Laboratory and Clinical Medicine, 82*(4), 649–655. https://doi.org/10.5555/uri:pii:0022214373900528

Li, X., Bai, Y., Jin, Z., & Svensson, B. (2022). Food-derived non-phenolic α-amylase and α-glucosidase inhibitors for controlling starch digestion rate and guiding diabetes-friendly recipes. In *, Vol. 153. LWT*. Academic Press. https://doi.org/10.1016/j.lwt.2021.112455.

Li, X., Wang, Y., Wu, J., Jin, Z., Dijkhuizen, L., Svensson, B., & Bai, Y. (2023). Designing starch derivatives with desired structures and functional properties via rearrangements of glycosidic linkages by starch-active transglycosylases. *Critical Reviews in Food Science and Nutrition*, 1–14. https://doi.org/10.1080/10408398.2023.2198604

Li, Y., Li, C., Gu, Z., Cheng, L., Hong, Y., & Li, Z. (2019). Digestion properties of corn starch modified by α-D-glucan branching enzyme and cyclodextrin glycosyltransferase. *Food Hydrocolloids, 89*, 534–541. https://doi.org/10.1016/j.foodhyd.2018.11.025

Liu, J., Meng, Y., Ma, A., & Chang, R. (2025). Digestion and fermentation of bionic grain-resistant corn starch and its effects on glucose response in mice. *npj science of food, 10* (3). https://doi.org/10.1038/s41538-025-00647-w

Liu, Z., Liu, X., Yu, J., Copeland, L., & Wang, S. (2023). Novel approach for quantitative characterization of short-range molecular order in gelatinized starch by X-ray diffraction. *Biomacromolecules, 24*(3), 1267–1273.

Mitchell, M. J., Billingsley, M. M., Haley, R. M., Wechsler, M. E., Peppas, N. A., & Langer, R. (2021). Engineering precision nanoparticles for drug delivery. *Nature Reviews Drug Discovery, 20*(2), 101–124.

Mohammad Amini, A., & Razavi, S. M. A. (2016). A fast and efficient approach to prepare starch nanocrystals from normal corn starch. *Food Hydrocolloids, 57*, 132–138. https://doi.org/10.1016/j.foodhyd.2016.01.022

Nsor-Atindana, J., Goff, H. D., Saqib, M. N., Chen, M., Liu, W., Ma, J., & Zhong, F. (2019). Inhibition of α-amylase and amyloglucosidase by nanocrystalline cellulose and spectroscopic analysis of their binding interaction mechanism. *Food Hydrocolloids, 90*, 341–352.

Nsor-Atindana, J., Yu, M., Goff, H. D., Chen, M., & Zhong, F. (2020). Analysis of kinetic parameters and mechanisms of nanocrystalline cellulose inhibition of α-amylase and α-glucosidase in simulated digestion of starch. *Food & Function, 11*(5), 4719–4731. https://doi.org/10.1039/d0fo00317d

Prasad, R., & Selvaraj, K. (2024). Choice of nanoparticles for theranostics engineering: Surface coating to nanovalves approach. *Nanotheranostics, 8*(1), 12.

Rao, J. P., & Geckeler, K. E. (2011). Polymer nanoparticles: Preparation techniques and size-control parameters. *Progress in Polymer Science (Oxford), 36*(7), 887–913. https://doi.org/10.1016/j.progpolymsci.2011.01.001

Salata, O. V. (2004). Applications of nanoparticles in biology and medicine. *Journal of Nanobiotechnology, 2*, 1–6.

Sankaran, K., Sivakami, S., Radhakrishnan, A. N., & Pandit, M. W. (1983). Studies on the size and shape of rabbit intestinal glucoamylase-maltase complex. *The Biochemical Journal, 213*(3), 719–725. https://doi.org/10.1042/bj2130719

Schäfer, B., Hecht, M., Harting, J., & Nirschl, H. (2010). Agglomeration and filtration of colloidal suspensions with DVLO interactions in simulation and experiment. *Journal of Colloid and Interface Science, 349*(1), 186–195.

Sharanagat, V. S., Saxena, D. C., Kumar, K., & Kumar, Y. (2023). Starch: Advances in modifications, technologies and applications. In *Starch: Advances in modifications, technologies and applications*. https://doi.org/10.1007/978-3-031-35843-2

Tian, Y., Liu, X., Kirkensgaard, J. J. K., Khakimov, B., Enemark-Rasmussen, K., Hebelstrup, K., … Zhong, Y. (2024). Characterization of different high amylose starch granules. Part I : Multi-scale structures and relationships to thermal properties. *Food Hydrocolloids, 146*, Article 109286. https://doi.org/10.1016/j.foodhyd.2023.109286

Tian, Y., Petersen, B. L., Liu, X., Li, H., Kirkensgaard, J. J. K., Enemark-Rasmussen, K., … Blennow, A. (2024). Characterization of different high amylose starch granules. Part II: Structure evolution during digestion and distinct digestion mechanisms. *Food Hydrocolloids, 149*(November 2023), Article 109593. https://doi.org/10.1016/j.foodhyd.2023.109593

Tian, Y., Wang, Y., Liu, X., Herburger, K., Westh, P., Møller, M. S., … Blennow, A. (2023). Interfacial enzyme kinetics reveals degradation mechanisms behind resistant starch. *Food Hydrocolloids, 140*, Article 108621. https://doi.org/10.1016/j.foodhyd.2023.108621

Tian, Y., Wang, Y., Zhong, Y., Møller, M. S., Westh, P., Svensson, B., & Blennow, A. (2023). Interfacial catalysis during amylolytic degradation of starch granules: Current understanding and kinetic approaches. *Molecules, 28*(9), 3799. https://doi.org/10.3390/molecules28093799%0A

Vieira, I. R. S., de Carvalho, A. P. A., & Conte-Junior, C. A. (2022). Recent advances in biobased and biodegradable polymer nanocomposites, nanoparticles, and natural antioxidants for antibacterial and antioxidant food packaging applications. *Comprehensive Reviews in Food Science and Food Safety, 21*(4), 3673–3716.

Vilaplana, F., & Gilbert, R. G. (2010). Characterization of branched polysaccharides using multiple-detection size separation techniques. *Journal of Separation Science, 33*(22), 3537–3554.

Wang, Y., Møller, M. S., & Svensson, B. (2024). Transglycosylase structures and their role in granular starch modification: A mini review. *Food Bioscience, 59*, 1–11. https://doi.org/10.1016/j.fbio.2024.104095

Wang, Y., Pang, C., Mohammad-Beigi, H., Li, X., Wu, Y., Lin, M. K. T. H., … Svensson, B. (2024). Sequential starch modification by branching enzyme and 4-α-glucanotransferase improves retention of curcumin in starch-alginate beads. *Carbohydrate Polymers, 323*, Article 121387. https://doi.org/10.1016/j.carbpol.2023.121387

Wang, Y., Tian, Y., Rennison, A. P., Blennow, A., Westh, P., Svensson, B., & Møller, M. S. (2025). Applying the Sabatier principle to decipher the surface-structure-dependent catalysis of different starch granules by pullulanase. *JACS Au, 5*, 55–60. https://doi.org/10.1021/jacsau.4c00932

Wu, Z., Zhang, X., Ma, M., Sui, Z., & Corke, H. (2026). The distribution of starch granule-associated proteins and their effects on starch properties: A review. *Food Hydrocolloids, 170*(June 2025), Article 111755. https://doi.org/10.1016/j.foodhyd.2025.111755

Xue, N., Wang, Y., Li, X., & Bai, Y. (2022). Enzymatic synthesis, structure of isomalto/malto-polysaccharides from linear dextrins prepared by retrogradation. *Carbohydrate Polymers, 288*, Article 119350. https://doi.org/10.1016/j.carbpol.2022.119350

Yan, X., Diao, M., Yu, Y., Gao, F., Wang, E., Wang, Z., Zhang, T., & Zhao, P. (2022). Characterization of resistant starch nanoparticles prepared via debranching and nanoprecipitation. *Food Chemistry, 369*, Article 130824.

Yang, J., Sun, Y., Dong, X., Li, M., Qin, Y., Dai, L., & Sun, Q. (2025). Interaction of starch nanoparticles with digestive enzymes and its effect on the release of polyphenols in simulated gastrointestinal fluids. *Food Chemistry, 472*(December 2024), Article 142883. https://doi.org/10.1016/j.foodchem.2025.142883

Yaskin Harush, M., Shani Levi, C., & Lesmes, U. (2025). Potential of process-induced modification of potato starch to modulate starch digestibility and levels of resistant starch type III. *Foods, 14*(5), 880.

Zhang, C., Wang, M., Tan, Z., Ma, M., Sui, Z., & Corke, H. (2023). Differential distribution of surface proteins/lipids between wheat A- and B-starch granule contributes to their difference in pasting and rheological properties. *International Journal of Biological Macromolecules, 240*(April), Article 124430. https://doi.org/10.1016/j.ijbiomac.2023.124430

Zhang, G., Ao, Z., & Hamaker, B. R. (2006). Slow digestion property of native cereal starches. *Biomacromolecules, 7*(11), 3252–3258.